Title
Radial Localization of Toroidicity-Induced Alfvén Eigenmodes

Journal
Physical Review Letters, 111(14)

ISSN
0031-9007

Authors
Wang, Zhixuan
□□□
Lin, Zhihong
et al.

Publication Date
2013-10-04

DOI
10.1103/physrevlett.111.145003

Radial Localization of Toroidicity-Induced Alfvén Eigenmodes

Zhixuan Wang (王直轩),[1] Zhihong Lin (林志宏),[1,*] Ihor Holod,[1] W. W. Heidbrink,[1] Benjamin Tobias,[2] Michael Van Zeeland,[3] and M. E. Austin[4]

[1]*University of California, Irvine, California 92697, USA*
[2]*Princeton Plasma Physics Laboratory, Princeton, New Jersey 08543-0451, USA*
[3]*General Atomics, San Diego, California 92186-5608, USA*
[4]*University of Texas, Austin, Austin, Texas 78712, USA*

(Received 13 June 2013; published 2 October 2013)

Linear gyrokinetic simulation of fusion plasmas finds a radial localization of the toroidal Alfvén eigenmodes (TAEs) due to the nonperturbative energetic particle (EP) contribution. The EP-driven TAE has a radial mode width much smaller than that predicted by the magnetohydrodynamic theory. The TAE radial position stays around the strongest EP pressure gradients when the EP profile evolves. The nonperturbative EP contribution is also the main cause for the breaking of the radial symmetry of the ballooning mode structure and for the dependence of the TAE frequency on the toroidal mode number. These phenomena are beyond the picture of the conventional magnetohydrodynamic theory.

DOI: 10.1103/PhysRevLett.111.145003 PACS numbers: 52.35.Bj, 52.55.Fa, 52.55.Pi, 52.65.Tt

Various Alfvén eigenmodes with discrete frequencies exist inside the spectral gap formed by the toroidal coupling in magnetically confined plasmas [1]. In particular, the toroidal Alfvén eigenmode (TAE) with radially extended structures can be driven unstable by pressure gradients of energetic particles (EPs) produced by fusion reactions and auxiliary heating [2]. These unstable Alfvén eigenmodes have been routinely observed in fusion experiments to induce a large EP transport [3–8], which could degrade overall plasma confinement and damage fusion devices. Therefore, better understanding of linear properties and nonlinear dynamics of the Alfvén eigenmodes is critical to the success of the burning plasma experiments such as ITER [9].

In the well-accepted and widely exercised paradigm, the growth rate of the Alfvén eigenmodes can be calculated from a perturbative EP contribution to a fixed mode structure and real frequency given by magnetohydradynamic (MHD) properties of thermal plasmas. However, kinetic effects of both EPs and thermal plasmas are important and should be treated on the same footing [10]. Gyrokinetic simulation, which averages out the rapid gyromotion of a charged particle about the magnetic field line while retaining wave-particle interactions and finite Larmor radius effects [11], has thus emerged as a necessary and powerful tool for studying the linear and nonlinear dynamics of Alfvén eigenmodes [10,12–19]. Recently, linear global gyrokinetic simulations of the reversed shear Alfvén eigenmodes have been verified and validated [20,21].

In the current work, the gyrokinetic toroidal code (GTC) [22–24] is used to simulate self-consistently the TAE mode structure and dispersion relation with realistic parameters of fusion plasmas. GTC linear simulation of the DIII-D tokamak experiment [6] finds a radial localization of the TAE due to the nonperturbative EP contribution. The EP-driven TAE has a radial mode width much smaller than that predicted by the MHD theory. The TAE radial structure peaks at and moves with the location of the strongest EP pressure gradients. Experimental data confirms that the eigenfunction drifts quickly outward in the radial direction. The nonperturbative EP contribution also breaks the radial symmetry of the ballooning mode structure and induces a dependence of the TAE frequency on the toroidal mode number, in excellent agreement with the experimental measurements.

The finding of the TAE radial localization is of conceptual and practical significance. Conceptually, the localization is beyond the conventional paradigm of the MHD theory with a perturbative treatment of the EP dynamics. Our finding blurs the boundary between the Alfvén eigenmodes and the energetic particle modes [25]. Practically, the radial localization could have profound implications on the EP transport. The radial mode width is one of the most important factors determining the EP transport level. The TAE radial drift could induce convective or even avalanchelike EP transport similar to that of the energetic particle modes [26].

Gyrokinetic simulation.—The equilibrium geometry and the plasma profiles used in the simulations are all taken from the self-consistent experimental equilibrium data at 525 ms of DIII-D shot no. 142111, constructed by EFIT [27] and ONETWO [28]. The equilibrium radial profiles are shown in Fig. 1. The magnetic shear is weakly reversed. The dominant TAE drive is the EP density gradients. The on-axis density and temperature are ($n_f = 2.93 \times 10^{18}\,\mathrm{cm}^{-3}$, $T_f = 24.5$ keV) for EPs, ($n_i = 2.65 \times 10^{19}\,\mathrm{cm}^{-3}$, $T_i = 1.64$ keV) for thermal ions, and ($n_e = 2.99 \times 10^{19}\,\mathrm{cm}^{-3}$, $T_e = 2.05$ keV) for electrons. At the steepest EP density gradient, $L_T = 1/(d\ln(T_f)/dr) \approx 52$ cm and $L_n = 1/(d\ln(n_f)/dr) \approx 9.8$ cm. The on-axis magnetic field is $B_a = 1.94$ T. The safety factor q denotes the ratio of toroidal to poloidal turns of the magnetic field line in a tokamak.

The on-axis ratio of the plasma pressure to the magnetic pressure is $\beta = \beta_e + \beta_i + \beta_{\rm EP} = 1.89\%$. The major radius is $R_0 = 176$ cm. The radial coordinate ρ in Fig. 1 is defined as the square root of the normalized toroidal flux $\rho \equiv \sqrt{\psi_{\rm tor}/\psi_{tw}}$, with $\psi_{\rm tor}$ being the toroidal flux and ψ_{tw} being the toroidal flux at the separatrix. Both thermal and energetic ions are deuterium. Since the background equilibrium does not change much during this short period (515–528 ms) [20,21], we use the same equilibrium data at $t = 525$ ms for all simulations except for a global translation of the q value, where the $q_{\rm min}$ value is calculated from the fitted equation $q_{\rm min} = 4 - 0.004(t - 528)$.

Both EPs and thermal ions are treated using the gyrokinetic equation in the current simulation. The electron drift kinetic equation is expanded to the second order using the fluid-kinetic hybrid electron model [21,29,30]. The boundary condition is assumed to be a perfect conducting wall. The choices of numerical parameters in simulations are based on convergence tests. We use 32 grid points in the parallel direction and 100 grid points in the radial direction. We keep the poloidal grid size approximately the same constant on different flux surfaces. Usually we use 30–35 grid points in one poloidal wavelength, with a grid size of about two thermal ion gyroradii. The time step size is $\Delta t \approx 0.1 R_0/v_{A0}$, where v_{A0} is the on-axis Alfvén speed. About 50 marker particles per cell are loaded for all species. The initial distribution of the marker particles is uniform in real space and Maxwellian in velocity space. A toroidal filter keeping only one toroidal mode number n is applied in the linear simulations. All poloidal harmonics are always kept. The simulation starts with the profiles in Fig. 1 as the initial conditions. The TAE grows exponentially from infinitesimal random noise.

Radial localization.—A direct comparison of the $n = 4$ TAE between simulation and experiment is shown in Fig. 2. The red lines (case 1) in both panels of Fig. 2 are the simulation results using the measured EP profile (see Fig. 1), while the black lines are the experimental measurements from electron cyclotron emission (ECE) [31] temperature fluctuation data. Using the best measured TAE structure in the electron cyclotron emission imaging (ECEI) window, we choose to compare experimental measurements at $t = 515$ ms with the simulation results with $q_{\rm min} = 4.052$. The frequency comparison is plotted in Fig. 2(a); the radial mode structure comparison is plotted in Fig. 2(b). In the simulation, we measure the frequencies in the plasma frame, but in the experiment the frequencies are measured in the lab frame, which are Doppler shifted. The observed plasma toroidal flow frequency is 1.9 kHz around the horizontal position $X = 2.05$ m, so the Doppler shift at the wave frequency is $1.9n$ kHz. All frequencies in Fig. 2(a) are in the plasma frame; i.e., the experimental values of the frequency have been subtracted by the Doppler shift. We find a good agreement between simulation results and experimental results in terms of the frequency. However, there are discrepancies in the radial locations of the eigenmode represented by the relative electron temperature perturbation $\delta T_e/T_e$ between simulation and ECE data from the experiment.

To resolve this discrepancy, we check the sensitivity of the mode location in the simulation to the EP density profile, which is the dominant drive for the instability and are also the most uncertain data experimentally. The results are summarized in case 2 and case 3 in Fig. 2, with the EP profile moved outside by 0.06 and 0.1 m, respectively. As shown in Fig. 2(a), three different simulations give eigenmodes with a frequency difference of only 1 kHz, or 1.5%, from each other. The frequency from the experiment (in the plasma frame) also lies just 3 kHz away. The major difference is the mode radial location. The mode locations are shown together with the EP density gradients in Fig. 2(b). We can see that the radial position of the TAE

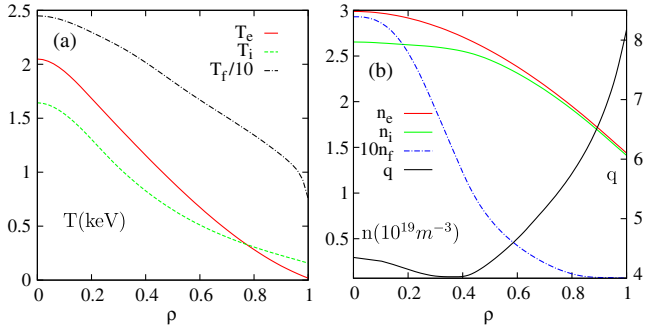

FIG. 1 (color online). Radial (ρ) profiles of (a) temperature T, (b) density n, and safety factor q of a DIII-D experiment (shot no. 142111 at 525 ms).

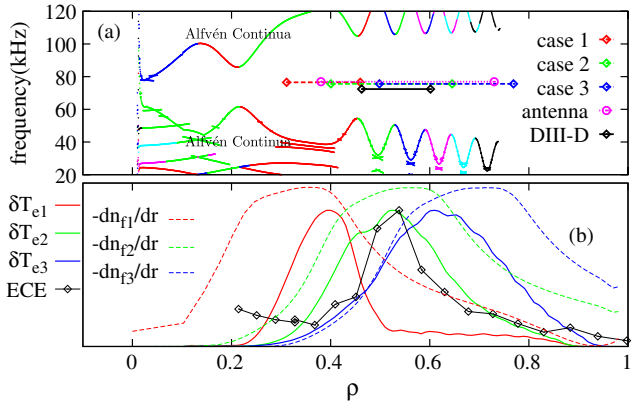

FIG. 2 (color online). (a) The frequencies (in the plasma frame) and locations (FWHM) of the simulated $n = 4$ TAE with different EP density profiles in the Alfvén continua. (b) A comparison of the mode radial structures with their corresponding EP drives. The solid lines are the rms values of the relative electron temperature perturbation $\delta T_e/T_e$; The dashed lines are the EP density gradient dn_f/dr values. Different colors indicate different EP profiles in the simulation. The black solid line is the ECE data of $\delta T_e/T_e$ from the DIII-D tokamak experiment.

depends strongly on the location of the strongest EP density gradients. The fact that the TAE radial eigenmode moves with the peak of the EP density gradients is inconsistent with the conventional picture of the MHD theory with perturbative treatment of EPs.

Without the presence of EPs, an artificial antenna is used to excite the weakly damped ideal MHD TAE by suppressing all kinetic effects in GTC simulations [14,15,19]. We find that the MHD TAE radial mode structure is independent of the radial location of the antenna source. Even though the MHD TAE eigenfrequency is about the same as the EP-driven TAE [see Fig. 2(a)], the radial extent of the MHD TAE is wider than that of the EP-driven unstable TAE. The antenna-excited ideal MHD TAEs of other toroidal mode numbers are all found to have broader radial ranges than their corresponding EP-driven unstable TAEs, which localize around the strongest EP pressure gradients. Therefore, the EP-driven TAE localizes around and moves with the peak of the EP density gradients.

Experimentally, the EP gradient is poorly determined. Measurements similar to those in Ref. [32] confirm that the EP transport is large and the profile is much flatter than the classical EP profile shown by the red dashed line in Fig. 2(b). Unfortunately, the resolution of the data is insufficient to detect variations in the EP gradient accurately. Nevertheless, fluctuation data provide indirect evidence of temporal shifts in the EP profile (see Fig. 3). In just 18 ms, the $n = 4$ radial eigenfunction shifts outward by 8 cm. During this interval, the $q = 4.5$ flux surface hardly changes, so changes in equilibrium alone cannot explain the outward migration of the TAE. The $n = 3$ TAE also shifts outward during this interval. It is hypothesized that a shift in the EP gradient similar to the modeled shift is responsible for the observed outward motion in ECE perturbation.

Nonperturbative EP contribution.—Among the three simulations in Fig. 2, the resultant mode radial location from case 2 fits the ECE data the best. The difference in the EP profiles between case 1 and case 2 is within the measurement uncertainty in DIII-D experiments. Therefore, all of the following simulations have been carried out with the EP density profile in case 2.

We note that the ideal MHD mode structure is calculated in a perturbative approach, where the EP pressure is ignored. However, the pressures of the EPs and thermal plasmas are comparable (as shown in Fig. 1) in typical tokamak experiments. Therefore, the mode structure and dispersion relation should be calculated self-consistently in a nonperturbative approach with the EP pressure and kinetic effects of all species taken into account.

A contour plot of the mode structure of $\delta T_e/T_e$ on a poloidal cross section from the GTC simulation is shown in Fig. 4, along with the ECE image at the same window. The eigenmode in the simulations has a typical ballooning structure [see Fig. 4(a)]. A series of m harmonics is seen together with similar radial profiles, each residing around its mode rational surface. They tend to have the same phase with neighbouring m harmonics on the low-field side, thus having an opposite phase with neighbouring m harmonics on the high-field side. The mode structure seen in the simulation agrees well with the experimental observation. The up-down symmetry of the ideal MHD mode structure is broken by the nonperturbative EP contribution, which introduces the radial symmetry breaking due to the radial variations of EP density gradients [6,10,14,15,19–21]. As a result, we can observe similar radial shearing of the mode structures in both simulation and experiment.

Further validation of the GTC simulations of localized TAEs due to nonperturbative EP contribution comes from the frequency agreement of various toroidal n modes. Simulation results of the TAE frequencies for different n numbers are summarized in Fig. 5. There are three major signals in the DIII-D experiment at this time: $n = 3$ TAE

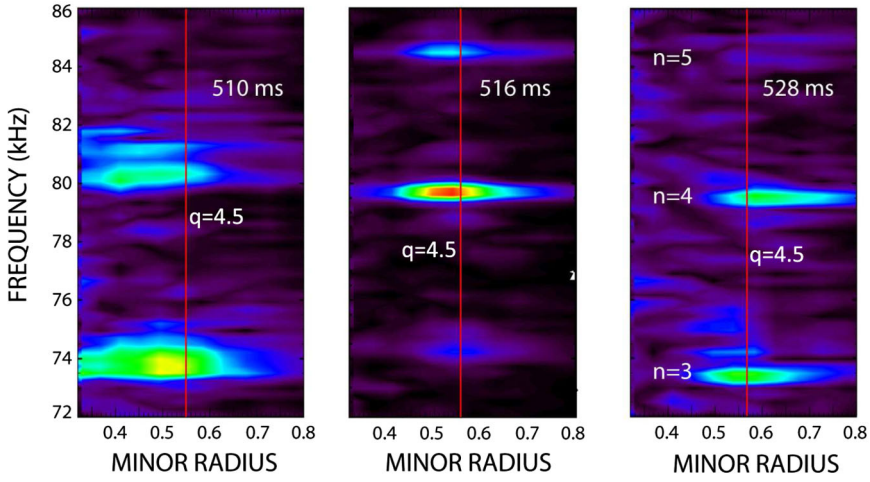

FIG. 3 (color online). Radial profiles of $\delta T_e/T_e$ frequency (in lab frame) spectra (in arbitrary unit) measured in the DIII-D experiment at $t = 510$ ms, 516 ms, and 528 ms, respectively. The vertical red lines indicate the location of the $q = 4.5$ flux surface at different times.

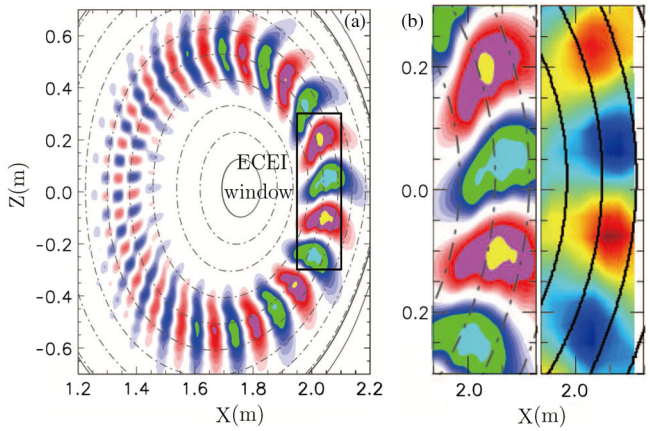

FIG. 4 (color online). (a) Contour plot of relative electron temperature perturbation $\delta T_e/T_e$ eigenstructure on a poloidal plane from GTC simulation. (b) Comparison of $\delta T_e/T_e$ structure from the simulation (left) and from the DIII-D experiment (right) in the ECEI window [the boxed region in (a)]. Red color represents positive perturbations and blue color represents negative perturbations.

with $f \approx 75$ kHz, $n = 4$ TAE with $f \approx 80$ kHz, and $n = 5$ TAE with $f \approx 85$ kHz [33]. These three signals from the experiment fit well with $n = 3, 4, 5$ TAE frequencies from GTC simulation results [see Fig. 5(a)]. The TAE frequencies are insensitive to the change in the q profile in both experiment and simulation [see Fig. 5(b)]. The difference in TAE frequencies between the simulation and experiment is about 5%–10% for these three toroidal modes. There are no experimental results to compare with the linear growth rates from simulations. However, the three major signals found in the experiment are the same as the three modes ($n = 3$, 4, 5) with the largest growth rates in the simulation.

GTC simulation in the ideal MHD limit shows that the ideal MHD TAE frequency is not sensitive to the toroidal

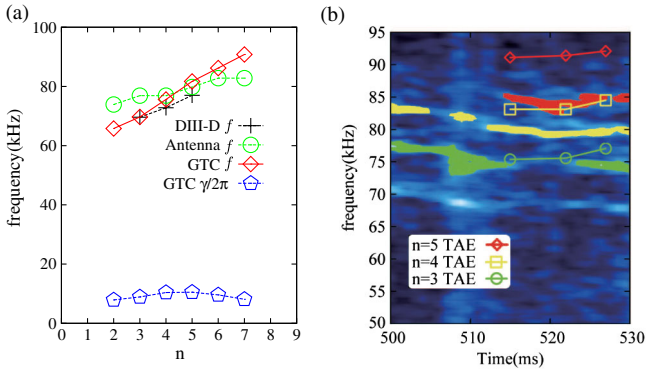

FIG. 5 (color online). (a) Comparison of EP-driven TAE frequencies and growth rates, for ideal MHD (with kinetic electrons) TAE frequencies observed in simulations, with TAE frequencies observed in DIII-D experiments, as a function of toroidal mode number n in the plasma frame at $t = 515$ ms; (b) TAE frequency as a function of time for $n = 3, 4, 5$ in the lab frame. Experiment data is the background, with $n = 3$, 4, 5 signals labeled with corresponding color. Dots and lines are simulation results.

TABLE I. $k_\theta \rho_{\mathrm{EP}}$ and $k_\theta \rho_d$ for different n modes.

n	1	2	3	4	5	6	7
$k_\theta \rho_{\mathrm{EP}}$	0.1	0.2	0.3	0.4	0.5	0.6	0.7
$k_\theta \rho_{\mathrm{d}}$	1.2	2.3	3.5	4.6	5.8	6.9	8.1

mode number, which is consistent with the prediction from the MHD theory [34]. When kinetic electrons are included, we found a higher antenna resonant frequency for a higher n number [green line in Fig. 5(a)] due to the trapped electron contribution. The kinetic effects of trapped electrons increase the frequencies by up to 10% and decrease the growth rates by about 20% compared to the simulation results using the fluid model. If we further include EPs, the slope is steeper [see the red line in Fig. 5(a)]. Similar frequency dependence on n number can also be found for experiment signals [see the black line in Fig. 5(a)]. This should also be attributed to the nonperturbative EP contribution, e.g., the EP diamagnetic flow effects. The EP diamagnetic flow angular frequencies at the peak of the EP density gradients are $\omega^*_{\mathrm{EP}} = 497n$ kHz, so $(1/2\pi)(n_f/n_i)\omega^*_{\mathrm{EP}} = 5n$ kHz. Therefore, the difference between the TAE frequencies of different n modes (about 4 kHz in the experiments and 6 kHz in the simulations) is about the same magnitude as the difference of their EP diamagnetic flow frequencies.

The $k_\theta \rho_{\mathrm{EP}}$ and $k_\theta \rho_d$ on the $q = 4.5$ flux surface for each n mode are listed in Table I. Here, the poloidal wave number $k_\theta = |\hat{b}_0 \times \nabla \delta\phi \cdot \nabla\psi|/(|\delta\phi||\nabla\psi|)$, and ρ_{EP} is the Larmor radius of the EPs. $\rho_d = q\rho_{\mathrm{EP}}/\sqrt{\epsilon}$ is the guiding center orbit width (i.e., the radial excursion of the guiding center trajectory in a tokamak), where $\epsilon = r/R_0$ is the inverse aspect ratio of the DIII-D tokamak. It suggests that other higher modes, which are not visible in experimental measurements, have smaller growth rates due to the stabilization effect of the large guiding center orbit width ρ_d and EP Larmor radius ρ_{EP}. All the TAE modes in Table I satisfy the following gyrokinetic ordering [11]: $\omega/\Omega_i \approx 0.5\%$–$0.7\% \ll 1$, $k_\parallel \rho_{\mathrm{EP}} \approx 0.4\% \ll 1$, $k_\perp \rho_{\mathrm{EP}} = 0.1$–$0.7$, where ω is the TAE frequency, Ω_i is the ion cyclotron frequency, and $k_\parallel$ and $k_\perp$ are the TAE perpendicular and parallel wavelength, respectively.

The authors acknowledge useful discussions with L. Chen, W. Deng, Y. Xiao, H. Zhang, and W. Zhang. This work is supported by the U.S. Department of Energy (DOE) SciDAC GSEP center. Simulations are performed using supercomputers at NERSC and ORNL.

*Corresponding author.
zhihongl@uci.edu

[1] C. Z. Cheng, L. Chen, and M. S. Chance, Ann. Phys. (N.Y.) **161**, 21 (1985).
[2] G. Y. Fu and J. W. Van Dam, Phys. Fluids B **1**, 1949 (1989).

[3] W. W. Heidbrink, E. J. Strait, E. Doyle, G. Sager, and R. T. Snider, Nucl. Fusion **31**, 1635 (1991).
[4] K. L. Wong *et al.*, Phys. Rev. Lett. **66**, 1874 (1991).
[5] K. Shinohara *et al.*, Nucl. Fusion **41**, 603 (2001).
[6] B. J. Tobias, I. G. J. Classen, C. W. Domier, W. W. Heidbrink, N. C. Luhmann, R. Nazikian, H. K. Park, D. A. Spong, and M. A. Van Zeeland, Phys. Rev. Lett. **106**, 075003 (2011).
[7] M. Podesta *et al.*, Nucl. Fusion **52**, 094001 (2012).
[8] Ph. Lauber, I. G. J. Classen, D. Curran, V. Igochine, B. Geiger, S. da Graça, M. García-Muñoz, M. Maraschek, and P. McCarthy, Nucl. Fusion **52**, 094007 (2012).
[9] http://www.iter.org/.
[10] H. S. Zhang, Z. Lin, and I. Holod, Phys. Rev. Lett. **109**, 025001 (2012).
[11] A. J. Brizard and T. S. Hahm, Rev. Mod. Phys. **79**, 421 (2007).
[12] Ph. Lauber, S. Gunter, and S. D. Pinches, Phys. Plasmas **12**, 122501 (2005).
[13] A. Mishchenko, R. Hatzky, and A. Konies, Phys. Plasmas **15**, 112106 (2008).
[14] W. Deng, Z. Lin, I. Holod, X. Wang, Y. Xiao, and W. Zhang, Phys. Plasmas **17**, 112504 (2010).
[15] H. S. Zhang, Z. Lin, I. Holod, X. Wang, Y. Xiao, and W. L. Zhang, Phys. Plasmas **17**, 112505 (2010).
[16] E. M. Bass and R. E. Waltz, Phys. Plasmas **17**, 112319 (2010).
[17] Y. Chen, S. E. Parker, J. Lang, and G.-Y. Fu, Phys. Plasmas **17**, 102504 (2010).
[18] X. Wang, F. Zonca, and L. Chen, Plasma Phys. Controlled Fusion **52**, 115005 (2010).
[19] W. Zhang, Z. Lin, and L. Chen, Phys. Plasmas **19**, 022507 (2012).
[20] D. A. Spong, E. M. Bass, W. Deng, W. W. Heidbrink, Z. Lin, B. Tobias, M. A. Van Zeeland, M. E. Austin, C. W. Domier, and N. C. Luhmann, Phys. Plasmas **19**, 082511 (2012).
[21] W. Deng, Z. Lin, I. Holod, Z. Wang, Y. Xiao, and H. Zhang, Nucl. Fusion **52**, 043006 (2012).
[22] Z. Lin, T. S. Hahm, W. W. Lee, W. M. Tang, R. B. White, Science **281**, 1835 (1998).
[23] W. Zhang, Z. Lin, and L. Chen, Phys. Rev. Lett. **101**, 095001 (2008).
[24] Y. Xiao and Z. Lin, Phys. Rev. Lett. **103**, 085004 (2009).
[25] L. Chen, Phys. Plasmas **1**, 1519 (1994).
[26] F. Zonca, S. Briguglio, L. Chen, G. Fogaccia, and G Vlad, Nucl. Fusion **45**, 477 (2005).
[27] L. L. Lao, H. St. John, R. D. Stambaugh, A. G. Kellman, and W. Pfeiffer, Nucl. Fusion **25**, 1611 (1985).
[28] W. W. Pfeiffer *et al.*, General Atomics Report No. GA-A16178, 1980 (unpublished).
[29] Z. Lin and L. Chen, Phys. Plasmas **8**, 1447 (2001).
[30] I. Holod, W. L. Zhang, Y. Xiao, and Z. Lin, Phys. Plasmas **16**, 122307 (2009).
[31] M. E. Austin and J. Lohr, Rev. Sci. Instrum. **74**, 1457 (2003).
[32] W. W. Heidbrink *et al.*, Phys. Rev. Lett. **99**, 245002 (2007).
[33] M. A. Van Zeeland *et al.*, Nucl. Fusion **52**, 094023 (2012).
[34] C. Z. Cheng and M. S. Chance, Phys. Fluids **29**, 3695 (1986).